Radiology

Virtual Unenhanced Images at Dual-Energy CT:
Influence on Renal Lesion Characterization

Mathias Meyer, MD • *Rendon C. Nelson, MD* • *Federica Vernuccio, MD* • *Fernando González, MD* •
Alfredo E. Farjat, PhD, MD • *Bhavik N. Patel, MD* • *Ehsan Samei, PhD* • *Thomas Henzler, MD* •
Stefan O. Schoenberg, MD • *Daniele Marin, MD*

From the Department of Radiology (M.M., R.C.N., F.V., F.G., D.M.) and Carl E. Ravin Advanced Imaging Laboratories (E.S.), Duke University Medical Center, 2301 Erwin Rd, Durham, NC 27710; Institute of Clinical Radiology and Nuclear Medicine, University Medical Center Mannheim, Medical Faculty Mannheim–Heidelberg University, Mannheim, Germany (M.M., T.H., S.O.S.); Section of Radiology, DIBIMED, University of Palermo, Palermo, Italy (F.V.); Department of Radiology, Clínica Alemana de Santiago, Universidad del Desarrollo, Santiago, Chile (F.G.); Department of Biostatistics and Bioinformatics, Duke University School of Medicine, Durham, NC (A.E.F.); and Department of Radiology, Stanford University, School of Medicine, Stanford, Calif (B.N.P.). Received May 8, 2018; revision requested July 12; revision received December 10; accepted January 24, 2019. **Address correspondence to** M.M. (e-mail: *mathias.myr@gmail.com*).

Conflicts of interest are listed at the end of this article.

Background: Dual-energy (DE) CT allows reconstruction of virtual noncontrast (VNC) images from a single-phase contrast agent–enhanced examination, potentially reducing the need for multiphasic CT to characterize renal lesions. However, data regarding diagnostic performance of VNC images for the characterization of renal lesions are limited.

Purpose: To determine whether renal mass CT performed by using VNC images allows for reliable identification of renal lesions and differentiation of contrast-enhanced from unenhanced lesions, compared with unenhanced images.

Materials and Methods: This is a retrospective study of 293 patients (105 women [mean age, 65 years; age range, 18–91 years] and 188 men [mean age, 66 years; age range, 23–90 years] with 379 renal lesions [craniocaudal diameter, 1.0–4.0 cm]) who underwent a single-energy unenhanced CT examination followed by a nephrographic-phase DE CT between June 2013 and October 2017 by using one of four different DE CT platforms from two vendors. VNC images were calculated by using vendor-specific algorithms. Each lesion was classified in a blinded and independent fashion by using the VNC or unenhanced image in combination with the nephrographic images. Attenuation measurements were obtained on the VNC, unenhanced, and nephrographic images. Unenhanced images and pathologic or imaging follow-up for more than 24 months served as reference standard.

Results: There was strong overall agreement between VNC and unenhanced images for renal lesion characterization (Cramer V = 0.85). VNC images yielded a high diagnostic performance (area under the receiver operating characteristic curve, 0.91; 95% confidence interval: 0.86, 0.95) for facilitation of differentiation of contrast-enhanced from unenhanced renal lesions. However, there was a reduction in diagnostic performance for depicting contrast-enhanced renal lesions by using VNC compared with unenhanced images (area under the receiver operating characteristic curve, 0.91 [95% confidence interval: 0.86, 0.95] vs 0.96 [95% confidence interval: 0.93, 0.99]; $P < .001$). Mean absolute difference between the VNC and unenhanced attenuation was 9.2 HU ± 8.7.

Conclusion: Virtual noncontrast images enabled accurate renal lesion characterization, albeit with a reduction in diagnostic performance for contrast-enhanced lesion characterization.

©RSNA, 2019

Online supplemental material is available for this article.

Exponential growth in medical cross-sectional imaging has led to an increase in the number of renal lesions incidentally detected at imaging. Many of these lesions are detected at examinations that are not tailored for optimal evaluation of a renal mass, thus leading to incomplete lesion characterization. As a consequence, current management guidelines recommend additional imaging for many of these lesions, typically in the form of a dedicated multiphasic renal mass CT protocol, which includes a noncontrast agent–enhanced CT examination (1).

Dual-energy (DE) CT allows for reconstruction of virtual noncontrast (VNC) images from a single-phase contrast-enhanced examination, which may eliminate the need for a multiphase CT protocol for the characterization of indeterminate renal lesions or a repeated dedicated imaging protocol in patients with incidentally

detected renal lesions (2). The two main benefits from the use of VNC images versus a separate unenhanced series are a reduction of the patient radiation burden by 30%–50% (depending on the number of imaging phases) and the elimination of any potential inaccuracies related to spatial misregistration (3,4). Although numerous phantom and human studies have advocated the routine adoption of VNC in place of unenhanced images, many institutions still perform an unenhanced examination as an integral part of CT protocols for the characterization of known or suspected renal lesions. The reasons for this reluctance to eliminate the unenhanced examination are likely multifactorial, including differences in noise texture and overall image appearance, susceptibility to artifacts, and reduced sensitivity for small calcifications on VNC images (4). More

Abbreviations

DE = dual energy, VNC = virtual noncontrast

Summary

Virtual noncontrast images enabled high diagnostic performance for renal lesion characterization. However, when compared with unenhanced images, there was a reduction in diagnostic performance for characterization of contrast agent–enhanced lesions.

Key Points

- Virtual noncontrast images yield high diagnostic performance (area under the curve, 0.91; 95% confidence interval: 0.86, 0.95; average error rate, 12%) for helping to differentiate contrast agent–enhanced from unenhanced renal lesions.
- Diagnostic performance is higher for unenhanced compared with virtual unenhanced images for differentiating contrast-enhanced from unenhanced renal lesions ($P < .001$).
- Whereas a higher error rate may be acceptable in the setting of incidentally discovered renal lesions, this decrease may not be acceptable for dedicated imaging of indeterminate renal lesions.

importantly, data regarding diagnostic performance of VNC images for the characterization of renal lesions are still limited to small case series that used early generation DE CT platforms (5–11).

We hypothesize that advances in DE CT technology (eg, better spectral separation, higher radiation tube output, advanced beam hardening correction, and improved material decomposition algorithms) led to substantial improvements in image quality and reliability of VNC images, which may allow for replacement of unenhanced with VNC images.

Thus, the purpose of this study was to determine whether VNC images allow for reliable differentiation of contrast-enhanced from unenhanced renal lesions and subsequent renal lesion characterization compared with unenhanced images.

Materials and Methods

This retrospective, single-center, Health Insurance Portability and Accountability Act–compliant study was approved by the institutional review board of Duke University (Durham, NC), and a waiver of written informed consent was obtained. One author of the study (R.N.) is a consultant for GE Healthcare (Waukesha, Wis). The other authors are not employees of or consultants for the industry and they had control of any data or information that might present a conflict of interest.

Patient Cohort

Figure 1 shows the patient accrual flowchart. A manual search was performed within the radiology picture archiving and communication system (Centricity 4.2; GE Healthcare) for patients who underwent a clinically indicated DE CT examination of the genitourinary system at our tertiary referral academic medical center between June 2013 and October 2017. Patients were eligible for inclusion if they underwent single-energy noncontrast CT followed by a contrast-enhanced DE CT of the kidney during the nephrographic phase, if at least one renal lesion with a craniocaudal diameter between 1.0 and 4.0 cm was manifest at imaging, and if they underwent previous or subsequent follow-

up imaging for at least 24 months. The 1.0-cm lower threshold was selected to avoid potential confounding from partial volume averaging in smaller renal lesions. Patients were considered ineligible for our study if the reference standard was inadequate; if the patient's total body weight was greater than 118 kg, which is our departmental cut-off for performing a DE CT examination; if metal artifacts from the spine or abdominal clips affected the kidney parenchyma; and/or if the patient had a known history of congenital or acquired multifocal cystic renal disease, or hereditary renal cancer syndromes.

A total of 458 patients fulfilled our inclusion criteria. The clinical indications for DE CT examination included the following: hematuria workup ($n = 229$), characterization of a known or suspected renal mass ($n = 215$), or active surveillance of a small renal mass in elderly or high-surgical-risk patients ($n = 14$). Of the 458 patients who were deemed initially eligible for our study, 165 were excluded from our target population because of missing DE data sets. Our final single-center retrospective study population was composed of 293 patients. The study patients are part of a large retrospective DE CT database, of which 85 patients have been reported in previously published studies (12–14) from our institution. In patients with multiple renal lesions ($n = 86$), up to five of the smallest lesions (≥ 1.0 cm) in each patient were included because small lesions represent the biggest challenge for characterization in clinical practice.

CT Examination Technique and Data Reconstruction

Patients underwent a CT examination for renal mass assessment performed on one of four DE CT scanners, including a single-energy noncontrast 120-kVp examination from the top of both kidneys through the pubic symphysis, followed by a DE contrast-enhanced examination during the nephrographic phase from the top of both kidneys to the iliac crest (Table E1 [online]).

Single-energy unenhanced images were reconstructed with a section thickness and interval of 2.5 mm by using a dedicated soft-tissue kernel. Contrast-enhanced DE CT images were generated from each manufacturer's software by using default settings with a section thickness and interval of 2.5 mm.

For each patient, the volume CT dose index, dose-length product, effective diameter, and size-specific dose estimate were recorded. The CT examination parameters and data reconstruction algorithms are in Appendix E1 (online).

Quantitative Image Analysis

Lesion attenuation values (in Hounsfield units) for the unenhanced, VNC, and contrast-enhanced 75-keV images were recorded by manually placing circular or ovoid regions of interest (Appendix E1 [online]). Lesion size, location within the kidney (ie, intraparenchymal vs partially or completely exophytic), renal lesion surrounding renal parenchyma attenuation, or distance to the proximity of the outer edge of the DE field of view were also recorded.

Lesion enhancement was measured by calculating the difference in attenuation (in Hounsfield units) between the contrast-enhanced and unenhanced images by using both unenhanced and VNC images. A change in Hounsfield units of greater than
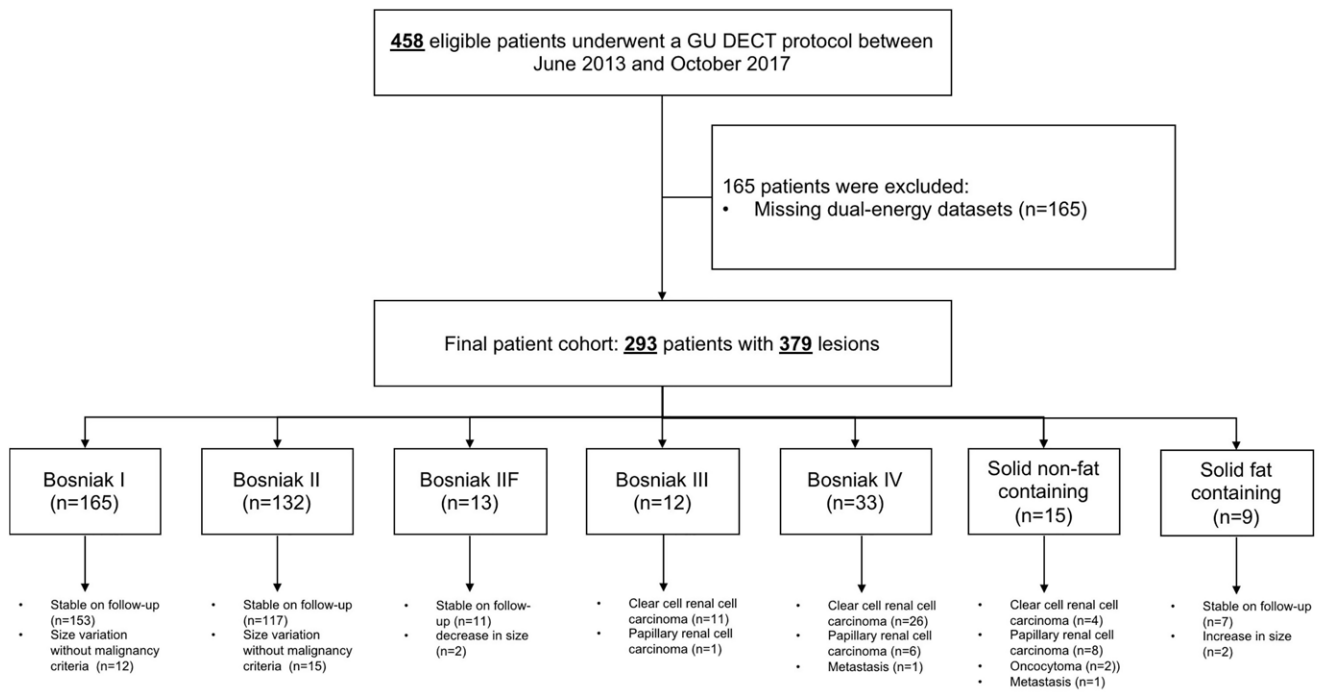
Figure 1: Flowchart of inclusion and exclusion criteria of the final patient cohort and the renal lesion characterization distribution. GU = genitourinary, DECT = dual-energy CT.

20 HU was used to determinate lesion enhancement of cystic or solid renal lesions (1). Renal lesions were also characterized on the basis of their attenuation properties on unenhanced images as fat-containing (<10 HU), unenhanced low-attenuation (between −10 and 20 HU), and unenhanced high-attenuation (>20 HU) lesions.

Qualitative Image Analysis

Four abdominal radiologists with different experience levels in genitourinary imaging (D.M., F.G., M.M., and F.V., with 8, 5, 4, and 1 years of experience, respectively) performed a renal lesion characterization. The Bosniak classification was used for cystic renal lesions, and grading regarding contrast-enhanced fat-containing and contrast-enhanced nonfat-containing solid renal lesions was used for noncystic renal lesions. Each reader independently interpreted each renal lesion in two reading sessions by using either the VNC images or the unenhanced images. The two reading sessions were separated by 4 weeks for each reader. During each reading session, readers were asked to classify renal lesions by using the unenhanced (either VNC or unenhanced) and contrast-enhanced images of each lesion in a side-by-side fashion. Appendix E1 (online) contains more details on the qualitative image reads.

On the basis of the assigned renal lesions category, renal lesions were divided into two different management categories as follows: Bosniak categories I and II, and enhanced fat-containing solid renal lesions were regarded as no additional management lesion because no additional management is recommended because of the low risk of malignancy; and Bosniak categories IIF, III, and IV, and contrast-enhanced nonfat-containing solid renal lesions were regarded as additional management lesions because additional follow-up or intervention is generally indicated.

The four readers were also asked to rank the quality of unenhanced and VNC images by using a five-point Likert scale on the basis of their overall perception of image quality, image noise, conspicuity of calcifications, and lesion visibility (Table E2 [online]).

### Clinical Reference Standard

Our clinical reference standard was established by a 4th-year radiology resident (M.M.) who had access to patient records, including pathologic reports and all images obtained before and after the index CT examination. Lesions were classified as benign or malignant on the basis of the reference standard as further detailed in Appendix E1 (online). For all renal lesions that could not be verified by using histologic examination, lesion stability was confirmed at follow-up with CT and MRI for a minimum of 24 months.

Statistical Analysis

Statistical analyses were performed by using software (R version 3.3.3, R Foundation for Statistical Computing, Vienna, Austria; and SAS version 9.4, SAS Institute, Cary, NC). The threshold for assessing statistical significance was an α level of .05.

Continuous variables were summarized as mean ± standard deviation, whereas categorical variables were reported as frequency counts with percentages from the total. Wilcoxon rank sum test and Fisher exact test were used to compare continuous demographic and CT radiation dose variables and categorical renal lesion variables among DE CT systems, respectively.

The quantitative analysis was performed to assess the agreement between the unenhanced and VNC attenuation values. The analysis included the sample Pearson moment
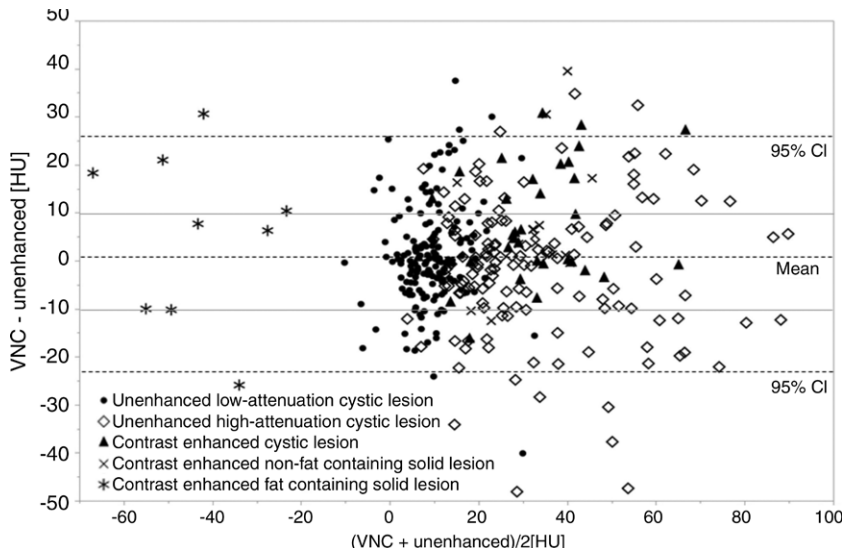
Figure 2: Bland-Altman plot for assessing the agreement between the measurements using the virtual noncontrast (VNC) attenuation values and unenhanced attenuation values. The horizontal dashed lines represent the mean (1.1 HU) and the limits of the 95% confidence interval (25.8 HU, −23.6 HU) for the difference.

correlation, the Bland-Altman plot (Fig 2), and a formal comparison between the VNC and unenhanced attenuation values, and absolute difference between the VNC and unenhanced attenuation among different DE CT systems by using the Wilcoxon signed rank test.

To evaluate the factors that are associated with existing discrepancies between the attenuation values measured on the VNC and unenhanced images, a multivariable analysis was performed. Appendix E1 (online) contains more details regarding how the multivariate analysis was performed. The receiver operating characteristic curves and the associated area under the receiver operating characteristic curve with 95% confidence interval were calculated for the enhancement calculation by using the VNC and unenhanced images by using the clinical reference standard as ground truth. The difference between the curves was evaluated by using the DeLong test for correlated curves.

Sensitivity and specificity for renal lesion enhancement for change in Hounsfield units of greater than 20 HU were estimated by using generalized linear mixed-effects models with threshold value as fixed effect and patients as random effects. The standard errors of the estimates were calculated by applying the Δ method and the corresponding 95% confidence intervals were obtained by inversely linking the confidence intervals on the linear scale.

In the qualitative analysis, several approaches were used to assess the agreement between unenhanced and VNC images and lesion characterization. For the qualitative image comparison of traits, the Wilcoxon rank sum test was used. To evaluate the agreement between unenhanced and VNC images on the basis of renal lesion characterization, the Cramer V statistic and Cochran-Mantel-Haenszel test were used. The Fleiss κ statistic was chosen to evaluate the interrater agreement for renal lesion characterization among the four readers in our study. For the Fleiss κ statistic interpretation, the recommendations by Landis and Koch (15) were chosen (poor, $\kappa < 0$; slight, $\kappa = 0$–0.20; fair, κ

= 0.21–0.40; moderate, κ = 0.41–0.60; substantial, κ = 0.61–0.80; and almost perfect, κ = 0.81–1).

Results

Baseline Demographics and CT Radiation Dose
We included 293 patients (105 women [mean age, 65 years $\pm$ 14; age range, 18–91 years] and 188 men [mean age, 66 years $\pm$ 13; age range, 23–90 years]) with 379 renal lesions. For the study population, the mean age was 65 years $\pm$ 13 (age range, 18–91 years), mean body weight was 82 kg $\pm$ 17 (range, 41–118 kg), and mean patient body mass index was 28 kg/m² $\pm$ 5 (range, 17–41 kg/m²). The mean patient effective diameter, calculated as the square root of the anteroposterior diameter multiplied by the transverse diameter, was 29.9 cm $\pm$ 3.6 (median, 29.8 cm; 25%–75% interquartile range, 27.7–32.5 cm). By omitting the unenhanced CT examination, on average a size-specific dose estimate reduction of 51% would have been achieved. This size-specific dose estimate reduction was higher for the dual-source DE CT system compared with the rapid kilovoltage-switching DE CT (65% vs 44%, respectively; $P < .01$). Patient demographics and CT radiation dose are summarized in Table 1.

Quantitative Image Analysis
Our data showed strong positive correlation between the VNC and unenhanced attenuation (in Hounsfield units) (ρ = 0.82; 95% confidence interval: 0.79, 0.85), with no difference between VNC and unenhanced images in mean attenuation for all renal lesions (20.3 HU $\pm$ 21.2 vs 19.2 HU $\pm$ 21.4, respectively; P = .10; Table E3 [online]). However, the absolute difference in attenuation between the VNC and unenhanced images was as high as 48.1 HU (Fig E3 [online]), with an average difference of 9.2 HU $\pm$ 8.7 for all renal lesions. Of note, we found a higher absolute difference between VNC and unenhanced images for unenhanced, high-attenuation lesions, compared with unenhanced low-attenuation lesions (11.6 HU $\pm$ 10.2 vs 7.4 HU $\pm$ 7.2; P = .001; Fig 3). The average absolute difference in attenuation between the VNC and unenhanced images was higher for the dual-source DE CT compared with the rapid-kilovolt-switching DE CT (10.5 HU $\pm$ 9.0 vs 7.3 HU $\pm$ 8.0, respectively; $P < .01$).

There was a reduction in area under the receiver operating characteristic curve for differentiating contrast-enhanced from unenhanced renal lesions by using VNC compared with unenhanced images (area under the receiver operating characteristic curve, 0.91 [95% confidence interval: 0.86, 0.95] vs 0.96 [95% confidence interval: 0.93, 0.99], respectively; $P < .01$). Similarly, specificity was lower by using the VNC compared with the unenhanced images (P = .002; Table 2). However, there was no change in sensitivity by using the VNC compared

Table 1: Patient Demographics, CT Radiation Dose, and Renal Lesions According to Dual-Energy CT System

Variable	Total	Dual-Source DE CT	Rapid-kilovolt-switching DE CT	P Value
Patients	293	174	119	
Patient age (y)*	65 ± 13	68 ± 11	65 ± 13	.20
Men (y)*	66 ± 13	66 ± 12	67 ± 13	.27
Women (y)*	65 ± 14	64 ± 15	68 ± 11	.38
No. of men (%)	188 (64.2)	101 (58.0)	79 (66.4)	.18
BMI (kg/m^2)*	28.1 ± 4.9	28.4 ± 4.8	27.5 ± 5.0	.11
Anterior-posterior diameter (cm)*	25.8 ± 4.1	26.0 ± 4.1	25.5 ± 4.0	.11
Transverse diameter (cm)*	34.7 ± 4.3	34.6 ± 4.1	34.7 ± 4.5	.74
Effective diameter (cm)*	29.9 ± 3.6	30.0 ± 3.8	29.7 ± 3.5	.48
CTDI$_{vol}$ unenhanced CT scan (mGy)*	11.8 ± 3.5	11.4 ± 2.7	12.7 ± 4.8	.15
CTDI$_{vol}$ enhanced DE CT scan (mGy)*	11.5 ± 3.9	9.7 ± 2.7	15.8 ± 3.0	<.001†
DLP unenhanced CT scan (mGy · cm)*	517.5 ± 183.3	485.2 ± 137.3	591.1 ± 247.7	.002†
DLP enhanced DE CT scan (mGy · cm)*	356.2 ± 143.5	294.2 ± 109.1	499.4 ± 108.9	<.001†
SSDE unenhanced CT scan (mGy)*	14.6 ± 3.5	14.2 ± 2.9	15.5 ± 4.7	.03†
SSDE enhanced DE CT scan (mGy)*	14.4 ± 5.1	12.0 ± 3.0	19.9 ± 4.5	<.001†
No. of patients with multiple lesions	86 (29.3)	54 (31.0)	32 (26.9)	.51
Two renal lesions	60 (20.5)	34 (19.5)	26 (21.8)	
Three renal lesions	19 (6.5)	15 (8.6)	4 (3.4)	
Four renal lesions	5 (1.7)	4 (2.3)	1 (0.8)	
Five renal lesions	2 (0.6)	1 (0.6)	1 (0.8)	
Total				
Renal lesions	379	228	151	.17
No. of contrast-enhanced solid lesions				
Fat containing	9 (2.4)	4 (1.8)	5 (3.3)	
Nonfat containing	15 (4.0)	11 (4.8)	4 (2.6)	
No. of cystic lesions				
Bosniak I	165 (43.5)	109 (47.8)	56 (37.1)	
Bosniak II	132 (34.8)	70 (30.7)	62 (41.1)	
Bosniak IIF	13 (3.4)	10 (4.4)	3 (2.0)	
Bosniak III	12 (3.2)	7 (3.1)	5 (3.3)	
Bosniak IV	33 (8.7)	17 (7.5)	16 (10.6)	

Note.—Unless otherwise indicated, data are frequency counts; data in parentheses are percentages. BMI = body mass index, CTDI$_{vol}$ = volume CT dose index, DE = dual energy, DLP = dose-length product, SSDE = size-specific dose estimation.

* Data are mean ± standard deviation.

† Statistically significant difference between dual-source, dual-energy CT and rapid-kilovolt-switching dual-energy CT.

with the unenhanced images for depicting contrast-enhanced lesions (P = .43; Table 2).

The average error rate of VNC images for depiction of enhancement was 12.1% (46 of 379), including 8.7% (33 of 379) false-positive and 3.4% (13 of 379) false-negative results. The average absolute difference in attenuation between VNC and unenhanced images was 17 HU for the false-positive results and 10 HU for false-negative results. A DE CT system comparison showed that the average error rate of VNC images for depiction of enhancement was similar between the dual-source DE CT and the rapid-kilovolt-switching DE CT (12.3% [28 of 228] vs 11.9% [18 of 151], respectively; P > .99), with again similar false-positive (8.3% [19 of 228] vs 9.3% [14 of 151], respectively; P = .52) and false-negative results (3.9% [nine of 228] vs 2.6% [four of 151]; P = .52).

Our multivariable analysis showed that absolute differences in attenuation between the VNC and unenhanced images were

influenced by multiple factors, including the unenhanced attenuation of the lesion (P < .01), the lesion's distance to the proximity of the outer edge of the DE field of view (P = .004), the patient's body size (P = .006), and the type of DE CT system (P = .01). Of note, the location of the lesion within the kidney had no effect (P = .35).

Qualitative Image Analysis

Our data showed strong overall agreement between VNC and unenhanced images for renal lesion characterization (Cramer V = 0.85). The general association between the metrics was strong after controlling for readers (Cochran-Mantel-Haenszel, P < .01). The average renal lesion characterization error rate of the VNC was 20.8% (79 of 379) per reader (range, 31–105 errors; Fig E4 [online]).

Interrater agreement was moderate to substantial for renal lesion characterization by using VNC and unenhanced
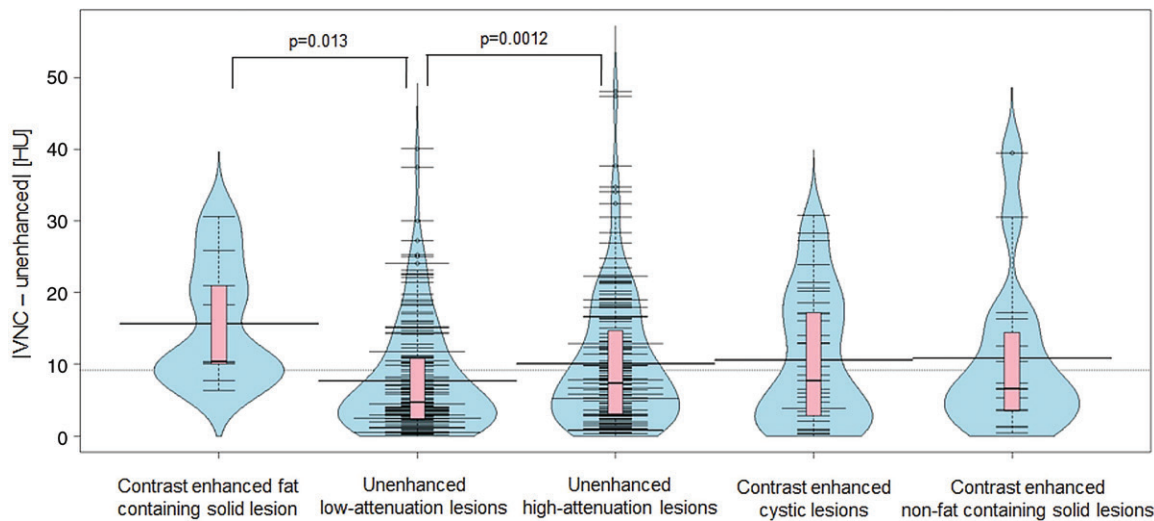
Figure 3: Beam plots and boxplots for the absolute value of the difference between virtual noncontrast (VNC)–unenhanced attenuation, indicating a statistical difference between unenhanced low-attenuation lesion and unenhanced high-attenuation lesions, and between contrast-enhanced fat-containing solid lesions and unenhanced high-attenuation lesions.

Table 2: Sensitivity and Specificity for Correct Lesion Characterization of Contrast-enhanced Lesions

Parameter	Value (%)	P Value
Sensitivity		
Virtual noncontrast images	79 (66, 88)	.43
Unenhanced images	85 (73, 93)	
Specificity		
Virtual noncontrast images	90 (86, 93)	.002
Unenhanced images	97 (94, 98)	

Note.—Data in parentheses are 95% confidence intervals. Clinical follow-up and/or intervention served as the reference standard. P value indicates difference between the unenhanced and virtual noncontrast images for attenuation changes greater than 20 HU.

images independently ($κ$ = 0.62 [95% confidence interval: 0.59, 0.65] and $κ$ = 0.60 [95% confidence interval: 0.57, 0.64], respectively). Of note, interreader agreement was only fair in the small subset (n = 13) of Bosniak IIF lesions for both VNC and unenhanced images ($κ$ = 0.28 vs $κ$ = 0.34, respectively; Table E4 [online]).

When lesions were categorized on the basis of their clinical management by using unenhanced images (the current standard of care), VNC images yielded unnecessary additional management recommendations for 12 Bosniak I and II lesions (range, three to 19 lesions for the four readers; Figs 4, 5, E5 [online]). However, VNC images did not indicate the need for additional management considerations in six lesions that were Bosniak category IIF or higher (range, one to 22 lesions for the four readers; Fig 6).

VNC images yielded worse overall image quality and noise scores compared with unenhanced images (P < .01 for both comparisons; Table 3). There was also a substantial reduction in the perceived visibility of subtle lesion calcifications on VNC images (overall mean detection rate by radiologists, 39% [13 of

33]; Fig 5). We found higher lesion visibility scores for VNC compared with unenhanced images (P < .01; Fig 4).

Discussion

Our study showed a strong agreement between VNC and unenhanced images for renal lesion characterization (Cramer V = 0.85). VNC images yielded high diagnostic performance (area under the receiver operating characteristic curve, 0.91; 95% confidence interval: 0.86, 0.95) in differentiating contrast-enhanced from unenhanced renal lesions, however, with a reduction compared with unenhanced images (area under the receiver operating characteristic curve, 0.96; 95% confidence interval: 0.93, 0.99; P < .001). The average error rate of VNC images for depiction of enhancement was 12.1% (46 of 379), which included an additional management recommendation error rate of 4.8% (18 of 379). Whereas these error rates may be acceptable in the setting of incidentally found renal lesions (such as a patient population in the emergency department), where additional costs and/or radiation burden from repeat imaging can be an issue, this decrease may not be acceptable for dedicated imaging of indeterminate renal lesions.

Results from previous studies (7,10,11,16–26) have demonstrated variable attenuation error rates of VNC images, with the majority of these studies demonstrating a good correlation between the VNC and the unenhanced attenuation values of various anatomic regions with differences below 5 HU. However, some studies (21,26,27) have shown differences between VNC and unenhanced attenuation values of up to 10 HU. Compared with our study, these studies were limited by smaller sample sizes, single-vendor analyses, renal lesion selection bias with lack of high-attenuation unenhanced renal lesions, and no genitourinary-specific imaging protocols (eg, DE portal venous phase or DE excretory phase imaging), which may not represent routine clinical practice.

The results of our multivariable analysis showed that unenhanced high attenuation in renal lesions, a shorter distance from
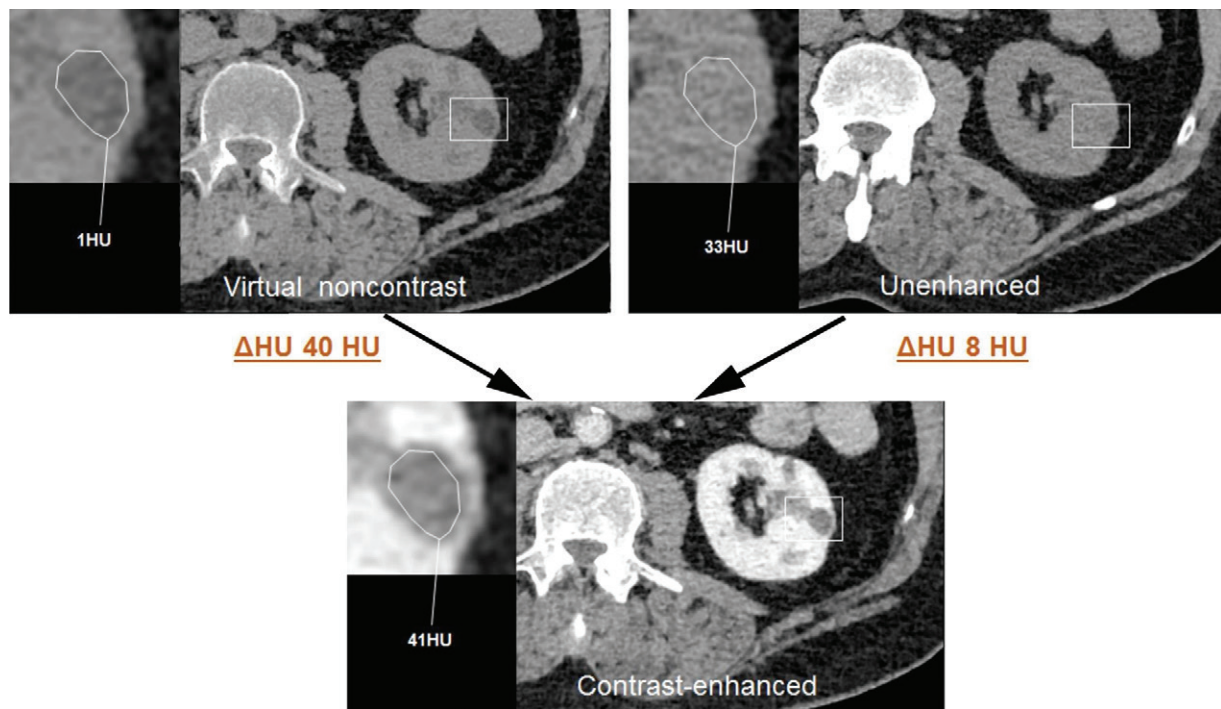
Figure 4: Images in a 61-year-old female patient with hematuria who underwent biphasic genitourinary dual-energy CT. In the contrast-enhanced axial image (bottom), a hypoattenuating renal lesion is displayed that appears hypoattenuating on the virtual non-contrast axial image (top left) and isoattenuating on the axial unenhanced image (top right). This mimics false-positive enhancement (contrast-enhanced nonfat-containing solid renal lesion) on the virtual noncontrast image in a true Bosniak II lesion (attenuation > 20 HU on unenhanced and no contrast enhancement on clinical follow-up imaging).

the proximity of the outer edge of the DE field of view, larger patient size, and type of DE CT system were found to have an effect on the absolute difference between VNC and unenhanced attenuation values. The influence of high attenuation in renal lesions, in particular in unenhanced high-attenuation renal lesions, is most likely linked to iron content, colloid formation, infection, or in a small portion of patients a retention of iodinated contrast material because of previous transient iodine accumulation (28). Iron content and colloid formation may have a DE ratio similar to that of iodine, whereas infection and transient iodine accumulation represent temporary true iodine uptake. The false assumption of iodine content with incorrect attenuation subtraction resulted in unenhanced high-attenuation lesions perceived as a solid low-enhanced renal lesion (eg, papillary renal cell carcinomas). Another influencing factor was proximity of the outer edge of the DE field of view. Lesions closer to the proximity of the outer edge of the DE field of view resulted in a greater difference in attenuation between the VNC and unenhanced images for the dual-source DE CT system. This emphasizes the importance of correct patient positioning for the dual-source DE CT systems. The negative effect of larger patient size on attenuation values is known (13,29) and is related to the beam-hardening and photon-starvation phenomena.

Although VNC images were rated as diagnostic, image quality and image noise were worse compared with the unenhanced images, which may further hamper the clinical acceptance of VNC images. These findings differ from previous studies, which demonstrated no difference in image quality between unenhanced

and VNC images when a second generation or newer DE CT system was used (10,16–26). The factors for this difference may be multifactorial, including different patient cohorts with different contrast media phases, patient size, and subjective image interpretations. However, in our study, this diminished image quality did not affect lesion characterization or enhancement measurements as lesion visibility improved.

We demonstrated a size-specific dose reduction on average of 51%, and this reduction was higher for the dual-source DE CT (65% vs 44%). This is in accordance with previous renal lesion imaging studies (6,11,12,17,30–32). However, approaches maintaining diagnostic performance should always precede dose reduction, as this may only lead to inconclusive examinations.

In addition to the retrospective single-center nature, some limitations of our study merited consideration. First, our reference standard included only a small proportion of lesions that underwent definitive characterization at pathologic analysis. We tried to overcome this limitation by including only patients with imaging follow-up of at least 24 months or patients with proven histologic workup. However, the 24 months follow-up interval chosen in this study may be too short because some contrast-enhanced masses may grow slowly and some Bosniak IIF lesions may increase in complexity after follow-up of 24 months. Thus, recent guidelines (1,33) recommend follow-up imaging for at least 36 months, and up to 60 months. Of note, Bosniak IIF lesions in our study cohort had at least 36 months follow-up and all contrast-enhanced lesions underwent a histologic workup. Second, for the dual-source DE CT, we deviated
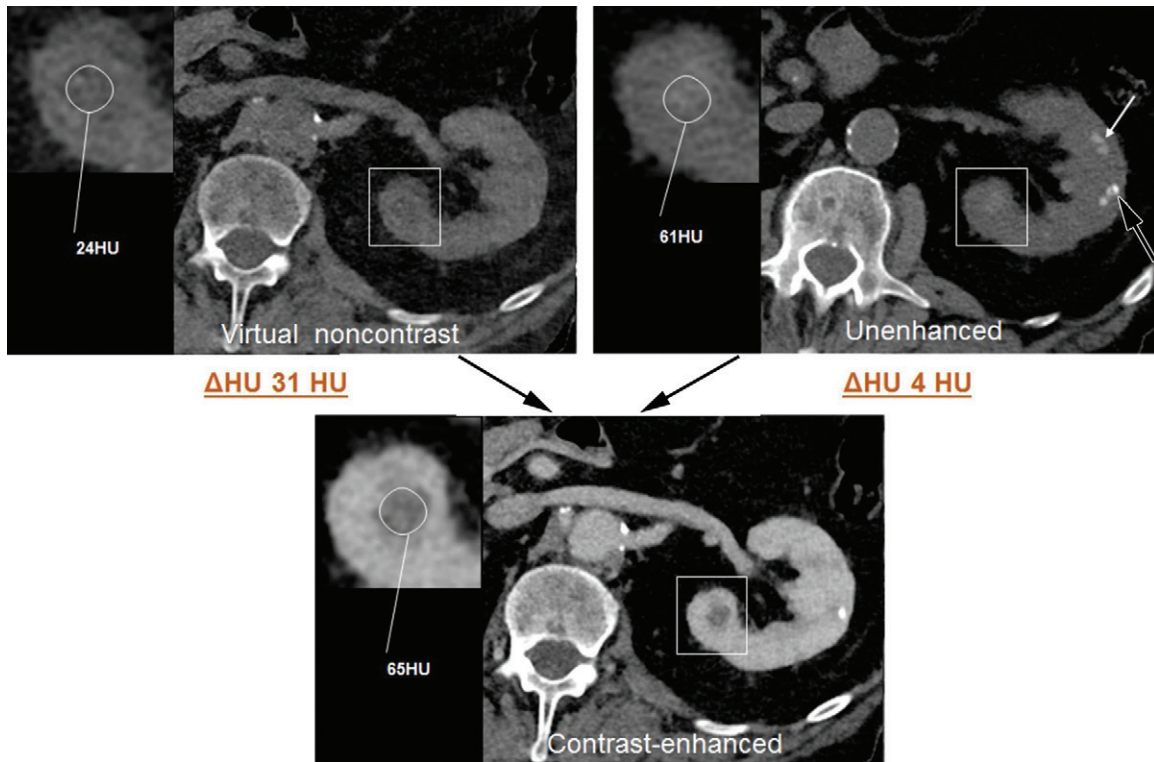
Figure 5: Images in a 71-year-old male patient with recurring hematuria undergoing biphasic genitourinary DE CT. In the contrast-enhanced axial image (bottom), a hypoattenuating renal lesion with isoattenuating contents is displayed (in box), which appears weakly hypoattenuating on the axial virtual noncontrast axial image (top left) and hyperattenuating on the axial unenhanced image (top right). This mimics false-positive contrast enhancement (ie, contrast-enhanced nonfat-containing solid renal lesion) in a true Bosniak II lesion (attenuation > 20 HU on unenhanced and no contrast enhancement at clinical follow-up imaging). There is a misregistration error between the unenhanced and contrast-enhanced image. The small lesion with hemorrhage (white arrow) and a calcification (black arrow) are not visible on the virtual noncontrast image.
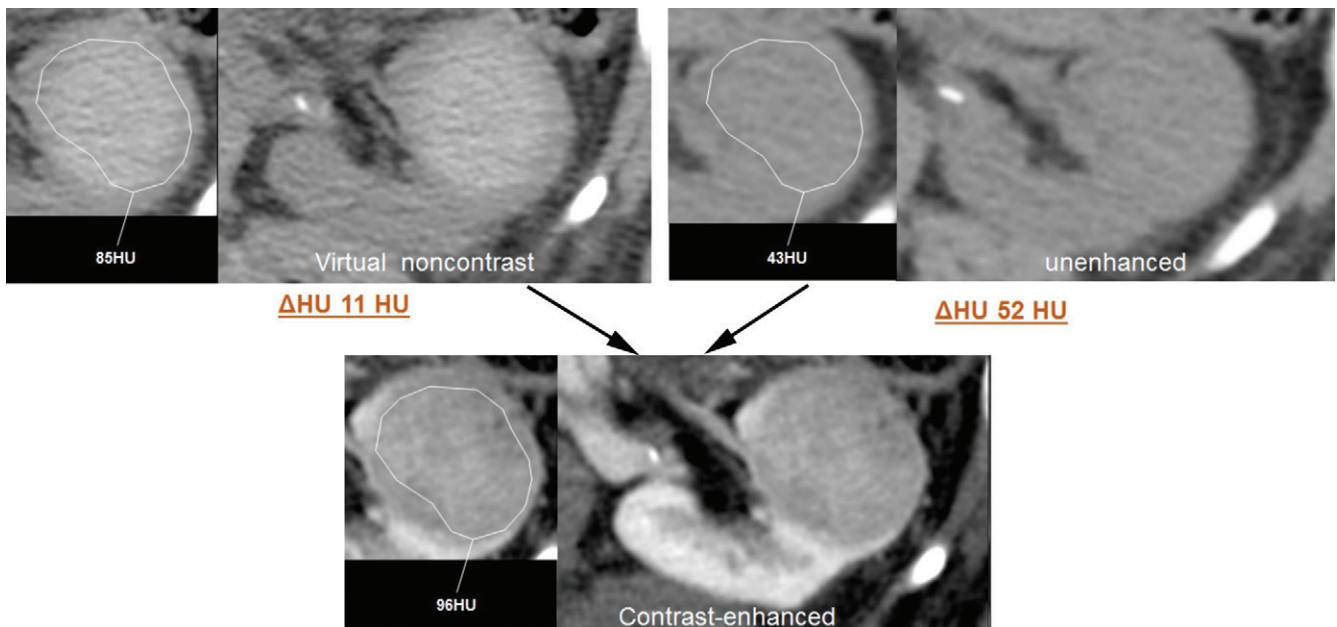
Figure 6: Images in a 74-year-old male patient with a mass suspected of hematuria who underwent biphasic genitourinary DE CT. In the axial contrast-enhanced image (bottom), a heterogeneous isoattenuating renal lesion with contrast-enhanced components appears hyperattenuating on the axial virtual noncontrast image (top left) and isoattenuating on the axial unenhanced image (top right). The iodine subtraction failed and mimics a false-negative unenhanced hemorraghic Bosniak II lesion in a true contrast-enhanced nonfat-containing solid renal lesion, which was confirmed at histologic analysis as an oncocytoma.

Table 3: Qualitative Image Analysis

Parameter	Virtual Noncontrast Image	Unenhanced Image	P Value
Image quality			<.001
Score 1	0 (0)	0 (0)	
Score 2	5 (0.3)	16 (1.1)	
Score 3	72 (4.8)	296 (13.2)	
Score 4	528 (34.8)	834 (55.0)	
Score 5	911 (60.1)	370 (24.4)	
Image noise			<.001
Score 1	0 (0)	1 (0)	
Score 2	20 (1.3)	51 (3.4)	
Score 3	220 (14.5)	667 (44.0)	
Score 4	749 (49.4)	658 (43.4)	
Score 5	527 (34.8)	139 (9.2)	
Lesion visibility			.02
Score 1	81 (5.3)	56 (3.7)	
Score 2	149 (9.8)	132 (8.7)	
Score 3	331 (21.8)	296 (19.5)	
Score 4	412 (27.2)	426 (28.1)	
Score 5	543 (35.8)	606 (40.0)	

Note.—Data are frequencies; data in parentheses are percentages. This is a virtual noncontrast and unenhanced image comparison on the basis of the distribution of image trait scores of all readers. The scale for the traits goes from 1 to 5, with higher scores indicating superior performance. Values are presented as frequencies and percentages in brackets. All *P* values indicated a significant difference between the virtual noncontrast and unenhanced values.

from manufacturer-recommended defaults for the scanner collimation of 32 × 0.6 mm and 64 × 0.6 mm; instead, we used the wider 64 × 0.6 mm and 96 × 0.6 mm for the second- and third-generation dual-source DE CT systems, respectively. The narrower beam width improves quantitative accuracy. However, we favored to maintain acquisition speed consistent between the unenhanced and contrast-enhanced DE CT examination. Third, for Bosniak IIF lesions there was only a fair agreement among the readers regardless of the approach chosen, indicating high interrater variability in these clinically challenging lesions, which may have led to an over- or underestimation of these renal lesions. Finally, our results do not apply to slow-kilovolt-switching and dual-layer DE CT systems, and radiologists should be careful to apply our findings to their own platforms. Nonetheless, our study included the two major DE CT platforms, which are the ones most commonly used in clinical routine.

In conclusion, we demonstrated a strong agreement of VNC and unenhanced images for renal lesion characterization. Our results showed a high diagnostic performance for differentiating contrast-enhanced from unenhanced lesions, with a reduction compared with unenhanced images. The average error rate of VNC images for the depiction of enhancement of 12% may be too high for dedicated renal mass protocols, and each individual institution should weigh the benefits of a DE CT protocol against the risks of a diagnostic performance drop.

References

1. Herts BR, Silverman SG, Hindman NM, et al. Management of the incidental renal mass on ct: a white paper of the ACR incidental findings committee. J Am Coll Radiol 2018;15(2):264–273.
2. Mileto A, Sofue K, Marin D. Imaging the renal lesion with dual-energy multidetector CT and multi-energy applications in clinical practice: what can it truly do for you? Eur Radiol 2016;26(10):3677–3690.
3. Mileto A, Marin D. Dual-energy computed tomography in genitourinary imaging. Radiol Clin North Am 2017;55(2):373–391.
4. Kaza RK, Ananthakrishnan L, Kambadakone A, Platt JF. Update of dual-energy CT applications in the genitourinary tract. AJR Am J Roentgenol 2017;208(6):1185–1192.
5. Cha D, Kim CK, Kim JJ, Park BK. Evaluation of hyperdense renal lesions incidentally detected on single-phase post-contrast CT using dual-energy CT. Br J Radiol 2016;89(1062):20150860.
6. Graser A, Becker CR, Staehler M, et al. Single-phase dual-energy CT allows for characterization of renal masses as benign or malignant. Invest Radiol 2010;45(7):399–405.
7. Graser A, Johnson TR, Hecht EM, et al. Dual-energy CT in patients suspected of having renal masses: can virtual nonenhanced images replace true nonenhanced images? Radiology 2009;252(2):433–440.
8. Kaufmann S, Sauter A, Spira D, et al. Tin-filter enhanced dual-energy-CT: image quality and accuracy of CT numbers in virtual noncontrast imaging. Acad Radiol 2013;20(5):596–603.
9. Kaza RK, Raff EA, Davenport MS, Khalatbari S. Variability of CT attenuation measurements in virtual unenhanced images generated using multimaterial decomposition from fast kilovoltage-switching dual-energy CT. Acad Radiol 2017;24(3):365–372.
10. Mileto A, Barina A, Marin D, et al. Virtual monochromatic images from dual-energy multidetector CT: variance in CT numbers from the same lesion between single-source projection-based and dual-source image-based implementations. Radiology 2016;279(1):269–277.
11. Neville AM, Gupta RT, Miller CM, Merkle EM, Paulson EK, Boll DT. Detection of renal lesion enhancement with dual-energy multidetector CT. Radiology 2011;259(1):173–183.
12. Marin D, Davis D, Roy Choudhury K, et al. Characterization of small focal renal lesions: diagnostic accuracy with single-phase contrast-enhanced dual-energy CT with material attenuation analysis compared with conventional attenuation measurements. Radiology 2017;284(3):737–747.
13. Mileto A, Allen BC, Pietryga JA, et al. Characterization of incidental renal mass with dual-energy CT: diagnostic accuracy of effective atomic number

maps for discriminating nonenhancing cysts from enhancing masses. AJR Am J Roentgenol 2017;209(4):W221–W230.

14. Schabel C, Patel B, Harring S, et al. Renal lesion characterization with spectral CT: determining the optimal energy for virtual monoenergetic reconstruction. Radiology 2018;287(3):874–883.

15. Landis JR, Koch GG. The measurement of observer agreement for categorical data. Biometrics 1977;33(1):159–174.

16. De Cecco CN, Muscogiuri G, Schoepf UJ, et al. Virtual unenhanced imaging of the liver with third-generation dual-source dual-energy CT and advanced modeled iterative reconstruction. Eur J Radiol 2016;85(7):1257–1264.

17. Faby S, Kuchenbecker S, Sawall S, et al. Performance of today's dual energy CT and future multi energy CT in virtual non-contrast imaging and in iodine quantification: A simulation study. Med Phys 2015;42(7):4349–4366.

18. Ho LM, Marin D, Neville AM, et al. Characterization of adrenal nodules with dual-energy CT: can virtual unenhanced attenuation values replace true unenhanced attenuation values? AJR Am J Roentgenol 2012;198(4):840–845.

19. Lee HA, Lee YH, Yoon KH, Bang DH, Park DE. Comparison of virtual unenhanced images derived from dual-energy CT with true unenhanced images in evaluation of gallstone disease. AJR Am J Roentgenol 2016;206(1):74–80.

20. Li Y, Li Y, Jackson A, et al. Comparison of virtual unenhanced CT images of the abdomen under different iodine flow rates. Abdom Radiol (NY) 2017;42(1):312–321.

21. Sahni VA, Shinagare AB, Silverman SG. Virtual unenhanced CT images acquired from dual-energy CT urography: accuracy of attenuation values and variation with contrast material phase. Clin Radiol 2013;68(3):264–271.

22. Tian SF, Liu AL, Wang HQ, Liu JH, Sun MY, Liu YJ. Virtual non-contrast computer tomography (CT) with spectral CT as an alternative to conventional unenhanced CT in the assessment of gastric cancer. Asian Pac J Cancer Prev 2015;16(6):2521–2526.

23. Wang W, Liu L, Zeng H, Sun C, Huang N, Zhang M. Utility of virtual unenhanced images and split-bolus injection using spectral multidetector CT for the assessment of renal cell carcinoma conspicuity and radiation dose. Int J Clin Pract 2016;70(Suppl 9B):B56–B63.

24. Wortman JR, Bunch PM, Fulwadhva UP, Bonci GA, Sodickson AD. Dual-energy CT of incidental findings in the abdomen: can we reduce the need for follow-up imaging? AJR Am J Roentgenol 2016;207(4):W58–W68.

25. Borhani AA, Kulzer M, Iranpour N, et al. Comparison of true unenhanced and virtual unenhanced (VUE) attenuation values in abdominopelvic single-source rapid kilovoltage-switching spectral CT. Abdom Radiol (NY) 2017;42(3):710–717.

26. Botsikas D, Triponez F, Boudabbous S, Hansen C, Becker CD, Montet X. Incidental adrenal lesions detected on enhanced abdominal dual-energy CT: can the diagnostic workup be shortened by the implementation of virtual unenhanced images? Eur J Radiol 2014;83(10):1746–1751.

27. Durieux P, Gevenois PA, Muylem AV, Howarth N, Keyzer C. Abdominal attenuation values on virtual and true unenhanced images obtained with third-generation dual-source dual-energy CT. AJR Am J Roentgenol 2018;210(5):1042–1058.

28. Silverman SG, Mortele KJ, Tuncali K, Jinzaki M, Cibas ES. Hyperattenuating renal masses: etiologies, pathogenesis, and imaging evaluation. RadioGraphics 2007;27(4):1131–1143.

29. Krauss B, Grant KL, Schmidt BT, Flohr TG. The importance of spectral separation: an assessment of dual-energy spectral separation for quantitative ability and dose efficiency. Invest Radiol 2015;50(2):114–118.

30. Ascenti G, Mazziotti S, Mileto A, et al. Dual-source dual-energy CT evaluation of complex cystic renal masses. AJR Am J Roentgenol 2012;199(5):1026–1034.

31. Mileto A, Marin D, Ramirez-Giraldo JC, et al. Accuracy of contrast-enhanced dual-energy MDCT for the assessment of iodine uptake in renal lesions. AJR Am J Roentgenol 2014;202(5):W466–W474.

32. Karlo C, Lauber A, Götti RP, et al. Dual-energy CT with tin filter technology for the discrimination of renal lesion proxies containing blood, protein, and contrast-agent. An experimental phantom study. Eur Radiol 2011;21(2):385–392.

33. Hindman NM, Hecht EM, Bosniak MA. Follow-up for Bosniak category 2F cystic renal lesions. Radiology 2014;272(3):757–766.